AUTOMATED TRACKING OF CELLS FROM PHASE CONTRAST IMAGES BY MULTIPLE HYPOTHESIS KALMAN FILTERS

Mengmeng Wang[1,2], *Lee-Ling Sharon Ong*[1], *Justin Dauwels*[1,2] *and H. Harry Asada*[1,3]

[1]Singapore-MIT Alliance for Research and Technology, Singapore 138602
[2]School of Electrical and Electronic Engineering, Nanyang Technological University, Singapore 639798
[3]Department of Mechanical Engineering, Massachusetts Institute of Technology, Cambridge, MA 02139, USA

ABSTRACT

Cell migration is a fundamental process for the development and maintenance of all multicellular organisms. Accurate cell tracking may lead to better interpretations of long-term cell behaviours. This paper describes an automated system to track multiple cells from experimental phase contrast images, which includes image registration, lumen segmentation, cell candidate detection, and multiple hypothesis Kalman filtering. We incorporate biological knowledge to associate the new observations to existing tracks. We apply our methodology to the problem of tracking endothelial cells in 3D angiogenic vessels. Numerical results indicate that our method associates cells more accurately compared to standard methods for cll association and tracking.

Index Terms— multiple hypothesis Kalman filters, cell tracking, phase contrast images, angiogenisis

1. INTRODUCTION

Cell migration is a fundamental process for the development and maintenance of all multicellular organisms. A better understanding of its mechanism may facilitate the investigation of novel therapeutic measures to control the cells. Manual cell tracking from in-vitro microscopy images is time-consuming, especially for large numbers of cells. Automated cell tracking is required to produce faster and more reliable analysis of long-term cell behavior from experimental data.

Angiogenesis is the growth process of blood vessels from existing vessels [1]. When exposed to Tumor Angiogenic Growth Factors (TAFs), endothelial cells (ECs) specialize into tip and stalk cells, migrate and proliferate to create a new vascular networks [2, 3]. We conduct angiogenic experiments in three-dimensional microfluidic devices [4]. The 3D vascular networks formed by the ECs is imaged over a period of 10 to 14 days with phase contrast microscopy; an approach commonly applied to observe long-term multicellular processes.

In this paper, we propose an automated image analysis system for multi-cell tracking from experimental phase contrast images. It includes image registration to align the phase contrast image sequences, lumen segmentation to represent lumen shape, cell detection to label cell candidates, and multiple hypothesis Kalman filtering to track the cell candidates in different frames.

In the following, we briefly describe the two common approaches to cell association and tracking. "Nearest-neighbourhood" association is the simplest cell association method, where each cell in one frame is associated with its spatially nearest cell in the subsequent frame [5, 6]. Another popular approach for cell tracking is to apply active contours, which evolves the cells in one frame in time to keep track of cell movements [7, 8, 9]. However, these two approaches fail when cell locations vary considerably between two successive frames due to the large time interval between frames, which is the case for our experimental data.

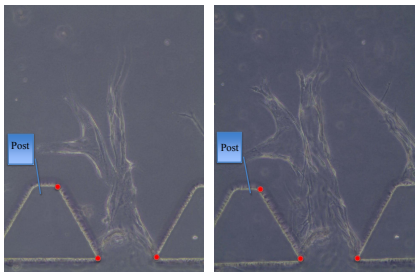

Fig. 1. Experimental phase contrast images of two successive frames. The trapezoidal posts are designed to retain the gel within the microfluidic channel.

Fig. 1 shows an example of our experimental phase contrast images for two successive frames, where the time interval is one day. Since the cells migrate a relative long distance, the existing association approaches will not work properly, as pointed out earlier. We propose backward Kalman filters with Multiple Hypothesis Tracking (MHT) for cell

This research was supported by the National Research Foundation Singapore through the Singapore MIT Alliance for Research and Technology's BioSystems and Micromechanics Inter-Disciplinary Research programme.

association and trajectory filtering, where two biology-based assumptions are incorporated. To our knowledge, we are the first to track cells forming 3D networks from experimental phase contrast images, and apply multiple hypothesis Kalman filters for cell association and trajectory filtering. Our numerical results suggest that this proposed approach significantly outshines standard methods for cell association and tracking.

This paper is structured as follows. In Section II, we explain our proposed multi-cell tracking system, which includes image registration, lumen segmentation, cell detection and multiple hypothesis Kalman filtering. In Section III, we present numerical results on our experimental phase contrast images. In Section IV, we offer concluding remarks.

2. AUTOMATED MULTI-CELL TRACKING SYSTEM

Fig. 2 illustrates the components of our automated multi-cell tracking system: image registration to align the image sequences, lumen segmentation to represent lumen shape, cell detection to label cell candidates and multiple hypothesis Kalman filtering. In the following, we will briefly discuss each component.

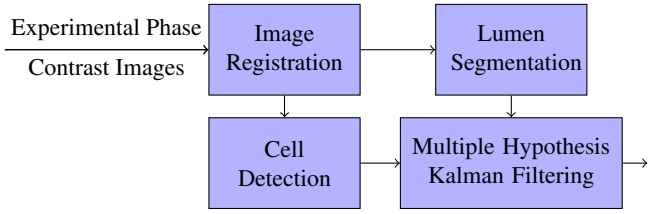

Fig. 2. Diagram of the proposed automated multi-cell tracking system.

2.1. Image Registration

Our experimental phase contrast image sequences are not aligned as they are acquired manually at different time, as shown Fig. 1. In order to integrate these images, they have to be registered into one common coordinate system.

Firstly, we determine the corresponding points between the images. We selected the red points in Fig. 1 as the corresponding points. The post edges are detected through Hough transform and represented by a set of lines. The corresponding points are the intersections of these lines. Then the images are translated and rotated, according to the relationship between the corresponding points, to align all images.

2.2. Lumen Segmentation

The aligned phase contrast images are then converted into binary images by thresholding. Lumen shape can be segmented through a series of morphological image processing steps, such as closing to fill the holes inside the lumen area, erosion to reduce noise size, and area opening to remove noise.

We represent the segmented lumen shape with Medial Axis Transforms (MATs), which are centerline coordinates and radii [10]. We can construct the original lumen shape from MATs for visualization.

2.3. Cell Detection

Cell candidates are detected from the aligned phase contrast images through template matching; we formulate this problem as a high-dimensional binary classification problem. In order to train the binary classifier, we manually extract a small set of cell and non-cell templates from the experimental phase contrast images, varying in size. To capture only texture information, we remove the size information by scaling all templates to the size 106×94, which is the mean size of all our original templates. The resulting scaled templates are converted to high-dimensional vectors $\mathbf{x}$, whose elements are the gray levels of the corresponding pixels. Next, each cell template is labeled as $y = +1$ and each non-cell template is labeled as $y = -1$. Our resulting training data contains $\mathbf{X} = [\mathbf{x}^1, \cdots, \mathbf{x}^N] \in \mathbb{R}^{m \times N}$ as input and $\mathbf{Y} = [y^1, \cdots, y^N] \in \mathbb{R}^{1 \times N}$ as output.

Since the feature dimension m is much larger than the template number N, it is imperative to extract a low-dimensional discriminative feature set that can predict the output data most effectively [11]. We apply Partial Least Square Regression (PLSR) for dimensionality reduction of the input data. Next, we train a binary classifier to distinguish cell and non-cell templates, leveraging on the extracted discriminative features. Through a sliding window approach, the cells are detected from the experimental phase contrast images by means of the trained classifier. The overall approach is summarized in Table 1.

Table 1. Cell detection algorithm.

Offline Training:
Input $\mathbf{X} \in \mathbb{R}^{m \times N}$ & $\mathbf{Y} \in \mathbb{R}^{1 \times N}$
PLSR Output: $\mathbf{Z} = \mathbf{V}^T\mathbf{X}$ & $\hat{\mathbf{Y}} = \mathbf{cZ}$
where $\mathbf{Z} \in \mathbb{R}^{m^* \times N}$, $\mathbf{V} \in \mathbb{R}^{m \times m^*}$, $\mathbf{c} \in \mathbb{R}^{1 \times m^*}$
Sliding Window Detection:
Test image: $\mathbf{T} = P \times Q$ matrix Template image: $p \times q$ matrix
for $i = \frac{p}{2} : P - \frac{p}{2}$ and $j = \frac{q}{2} : Q - \frac{q}{2}$
$\mathbf{T}_{\text{temp}} = \mathbf{T}(i - \frac{p}{2} + 1 : i + \frac{p}{2}, j - \frac{q}{2} + 1 : j + \frac{q}{2})$
$\mathbf{T}'_{\text{temp}} = \text{reshape}(\mathbf{T}_{\text{temp}}, m, 1)$
Cell Detection Criteria: $\mathbf{z} = \mathbf{V}^T\mathbf{T}'_{\text{temp}}$ and $\hat{\mathbf{Y}}(i,j) = \mathbf{cz}$
$\begin{cases} \text{Cell} & \text{if } \hat{\mathbf{Y}}(i,j) > 0 \\ \text{Non-Cell} & \text{Otherwise} \end{cases}$

In order to determine the optimal number m^* of PLS components (cf. Table 1), we monitor the percentage variance explained in the output variables. Our goal is to achieve 95% of the variance explained in the output variables with the smallest possible number of PLS components. In our numerical experiments, this leads to the setting $m^* = 4$. Following this automated approach, we label cell candidates in each frame in an automated manner.

2.4. Multiple Hypothesis Kalman Filtering

We combine backward Kalman filter with Multiple Hypothesis Tracking (MHT) to associate and filter the extracted cell candidates. At the end of our experiments, we fix and stain the nuclei and acquire confocal images. These images provide more accurate cell locations and hence, we use these coordinates as our initial condition and apply backward Kalman filtering. We denote the cell state for an individual cell (track) at time k by $\mathbf{x}_k = [x_k, y_k, \dot{x}_k, \dot{y}_k]^T$, which includes a two-dimensional cell position and velocity, and $\mathbf{P}_k$ is the covariance. The observation state is the two-dimensional cell position $\mathbf{z}_k = [x_k, y_k]^T$. The flowchart of our multiple hypothesis Kalman filtering system is shown in Fig. 3. From the initial tracks (end point observations of cell from confocal images), we recursively update the the individual cell states, system covariance and probability of a track with observations at each time step.

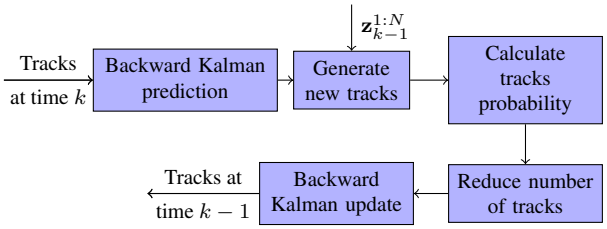

Fig. 3. Flowchart of multiple hypothesis Kalman filtering.

2.4.1. Backward Kalman Prediction

For each track at time k, we firstly predict the priori cell state estimate $\hat{\mathbf{x}}_{k-1|k}$ and system covariance estimate $\mathbf{P}_{k-1|k}$ using standard backward Kalman prediction:

$$\hat{\mathbf{x}}_{k-1|k} = \mathbf{F}\hat{\mathbf{x}}_{k|k}, \tag{1}$$

$$\mathbf{P}_{k-1|k} = \mathbf{F}\mathbf{P}_{k|k}\mathbf{F}^T + \mathbf{Q}, \tag{2}$$

where $\mathbf{F}$ is the state transition model, and $\mathbf{Q}$ is the covariance matrix of the process noise. Specifically, we have

$$\mathbf{F} = \begin{bmatrix} 1 & 0 & \Delta t & 0 \\ 0 & 1 & 0 & \Delta t \\ 0 & 0 & 1 & 0 \\ 0 & 0 & 0 & 1 \end{bmatrix}, \tag{3}$$

where $\Delta t = 1$ day.

2.4.2. Tracks Probability Generation

The next step is to generate new tracks and their probabilities. One track i at time k might be due to the migration or proliferation of an existing cell j at time $k-1$, or a new cell migrating into the gel from monolayer.

In this paper, we employ the Normalized Innovation Covariance (NIC) d^2 between track i and observation j as the validation gate to determine whether to generate a new track. The validation gate is calculated as follows:

$$d_{ij}^2 = \tilde{\mathbf{y}}_{ij,k-1}^T \mathbf{S}_{ij,k-1}^{-1} \tilde{\mathbf{y}}_{ij,k-1}, \tag{4}$$

where $\tilde{\mathbf{y}}_{ij,k-1}$ is the error (referred as the innovation) between the back-predicted observation i and the actual observation j, and $\mathbf{S}_{ij,k-1}$ is the corresponding innovation covariance. These quantities are computed as follows:

$$\tilde{\mathbf{y}}_{ij,k-1} = \mathbf{z}_{j,k-1} - \mathbf{H}\hat{\mathbf{x}}_{k-1|k}, \tag{5}$$

$$\mathbf{S}_{ij,k-1} = \mathbf{H}\mathbf{P}_{k-1|k}\mathbf{H}^T + \mathbf{R}, \tag{6}$$

where $\mathbf{H} = \begin{bmatrix} 1 & 0 & 0 & 0 \\ 0 & 1 & 0 & 0 \end{bmatrix}$ is the observation model which maps the state space into the observed space, and $\mathbf{R}$ is the covariance of the observation noise. The validation gate is used to generate the probability that new track i is associated with observation j by:

$$p_i(\mathbf{z}_{k-1}^j) \propto |2\pi\mathbf{S}_{ij,k-1}|^{-\frac{1}{2}} \exp^{-\frac{1}{2}d_{ij}^2}. \tag{7}$$

We assume that the cells nearer to the monolayer (larger y-position) are more likely to be new tracks. This probability is estimated as:

$$p_i(\mathrm{NT}) \propto \frac{1}{(a_1 - y_{k-1|k})^{a_2}}, \tag{8}$$

where a_1 and a_2 are the empirical parameters tuned from our experimental data, $y_{k-1|k}$ is the cell position in y-direction from backward Kalman prediction.

The tracks with low probability are discarded in order to limit the computational complexity. In addition, we include biological knowledge to reduce the number of the new tracks in each step. Since the doubling time of our ECs is 15 to 48 hours, we assume that one cell can at most split once within one day. In other words, we allow at most two cells at time k to be associated with one same cell at time $k-1$ during merging. In this way, the number of new tracks is reduced.

2.4.3. Kalman Update

We perform the backward Kalman update for the new tracks as follows:

$$\hat{\mathbf{x}}_{k-1|k-1} = \hat{\mathbf{x}}_{k-1|k} + \mathbf{K}_{k-1}[\mathbf{z}_{k-1} - \mathbf{H}\hat{\mathbf{x}}_{k-1|k}], \tag{9}$$

$$\mathbf{P}_{k-1|k-1} = (\mathbf{I} - \mathbf{K}_{k-1}\mathbf{H})\mathbf{P}_{k-1|k}, \tag{10}$$

where $\mathbf{K}_{k-1}$ is the optimal Kalman gain matrix that yields the minimum mean square error:

$$\mathbf{K}_{k-1} = \mathbf{P}_{k-1|k}\mathbf{H}^T(\mathbf{H}\mathbf{P}_{k-1|k}\mathbf{H}^T + \mathbf{R})^{-1}. \tag{11}$$

We can obtain the cell state estimates $\hat{\mathbf{x}}_{k-1|k-1}$ and system covariance estimates $\mathbf{P}_{k-1|k-1}$ for all the new tracks at time $k-1$. Then each of these new tracks is considered independently and used to generate new predictions for the next time step. We repeat this tracking process until $k = 1$.

Lastly, the hypothesis with maximum probability is selected as the tracking result.

3. RESULTS

We applied the proposed automated multi-cell tracking system to track the nuclei of endothelial cells in the 3D angiogenic sprouts from phase contrast image sequences.

There are four outcomes for a given classifier and set of instances: True Positive (TP), False Positive (FP), True Negative (TN) and False Negative (FN). To evaluate the performance of our PLSR cell detection approach quantitatively, precision and recall measures are estimated based on:

$$\text{Precision} = \frac{\text{TP}}{\text{TP+FP}} \quad \text{and} \quad \text{Recall} = \frac{\text{TP}}{\text{TP+FN}}. \qquad (12)$$

The ground truth is obtained by manually extracting the cells from the confocal images. The value for the precision is 88.11% and for the recall is 80.83% respectively, indicating that PLSR is able to detect most of the cells correctly.

We provide examples of association results from the proposed multi-cell tracking system in Fig. 4(a) and 4(b). We also apply backward Kalman filter with validation gating for cell association, as shown in Fig. 4(c) and 4(d). We can see that the proposed multi-cell tracking approach produces better tracking results than backward Kalman filter with validation gating.

In Table 2, we compare the accuracy of the proposed approach for cell association with the commonly used "nearest-neighbourhood" approach and backward Kalman filter with validation gating. We obtained the ground truth through manual association, which is the traditional method of analyzing the cell migratory behaviours. Since the time interval between frames is one day, cells migrate over a relatively long distance between frames. In "nearest-neighbourhood" association, the new tracks at time k are always associated wrongly to cells that are near to the monolayer at time $k-1$. However, by predicting the track backwards each time step via a constant velocity motion model, we are more likely to associate the correct observations to tracks with the backward Kalman filter. Therefore the association accuracy improves from 27.34% from 60.16% for the Kalman filter association. In our approach, we combine multiple hypothesis tracking with backward Kalman filter, which allows delay decision as more information become available. Moreover, biological knowledge is incorporated when considering the new cells from the monolayer and reducing the number of new tracks. As a result, we can track not only the migration and proliferation of the existing cells but also the new cells from monolayer and out-of-focus plane. This explains why the association accuracy increases to 85.94% for our approach.

Table 2. Cell association accuracy for different approaches.

	Correct associations	Total associations	Association accuracy
Nearest-neighbourhood association	35	128	27.34%
Kalman filter with validation gating	77	128	60.16%
Kalman filter with MHT	110	128	85.94%

4. CONCLUSION

We presented a multi-cell tracking system by combining multiple hypothesis tracking with backward Kalman filters; we applied this system to track the nuclei of ECs in 3D angiogenic sprouts from phase contrast image sequences. Biological knowledge is included when calculating the probability and reducing the number of new tracks. The numerical results suggest that our proposed system generates more accurate associations than "nearest-neighbourhood" association approach and backward Kalman filter with validation gating.

In future work, the lumen shape can be incorporated to constrain the cell velocity during association, in order to further improve the tracking accuracy.

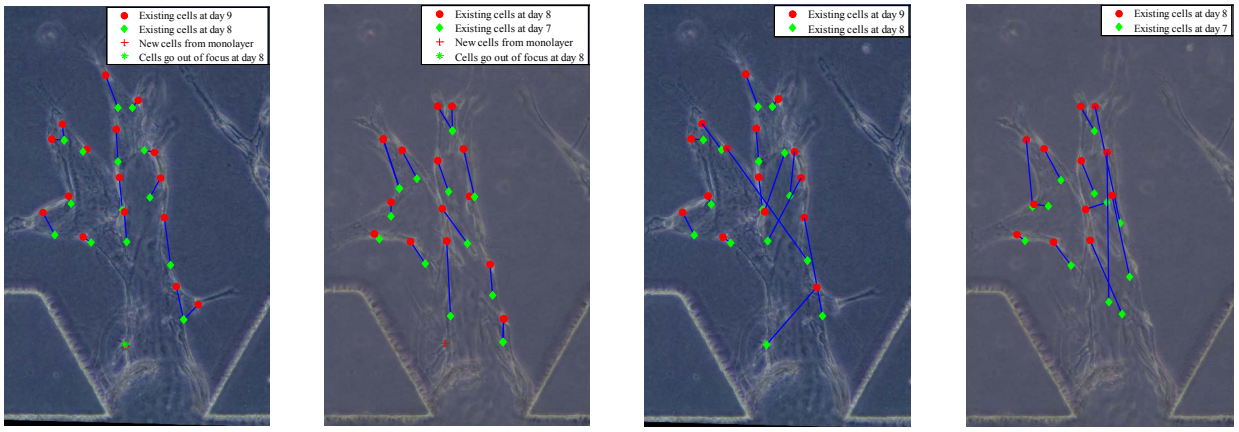

(a) Day 9 to day 8 (Kalman filter with MHT)

(b) Day 8 to day 7 (Kalman filter with MHT)

(c) Day 9 to day 8 (Kalman filter with validation gating)

(d) Day 8 to day 7 (Kalman filter with validation gating)

Fig. 4. Cell tracking results: (a) and (b) use backward Kalman filter with MHT (85.94% association accuracy); (c) and (d) use backward Kalman filter with validation gating (60.16% association accuracy); each image presents the tracking results for two successive frames; the background is the experimental phase contrast image.

5. REFERENCES

[1] H. Gerhardt, "Vegf and endothelial guidance in angiogenic sprouting," *VEGF in Development*, pp. 68–78, 2008.

[2] A. Das, D. Lauffenburger, H. Asada, and R.D. Kamm, "A hybrid continuum–discrete modelling approach to predict and control angiogenesis: analysis of combinatorial growth factor and matrix effects on vessel-sprouting morphology," *Philosophical Transactions of the Royal Society A: Mathematical, Physical and Engineering Sciences*, vol. 368, no. 1921, pp. 2937–2960, 2010.

[3] F. De Smet, I. Segura, K. De Bock, P.J. Hohensinner, and P. Carmeliet, "Mechanisms of vessel branching filopodia on endothelial tip cells lead the way," *Arteriosclerosis, thrombosis, and vascular biology*, vol. 29, no. 5, pp. 639–649, 2009.

[4] W.A. Farahat, L.B. Wood, I.K. Zervantonakis, A. Schor, S. Ong, D. Neal, R.D. Kamm, and H.H. Asada, "Ensemble analysis of angiogenic growth in three-dimensional microfluidic cell cultures," *PloS one*, vol. 7, no. 5, pp. e37333, 2012.

[5] Z. N. Demou and L. V. McIntire, "Fully automated three-dimensional tracking of cancer cells in collagen gels determination of motility phenotypes at the cellular level," *Cancer Research*, vol. 62, no. 18, pp. 5301–5307, 2002.

[6] X. Chen, X. Zhou, and S. T. Wong, "Automated segmentation, classification, and tracking of cancer cell nuclei in time-lapse microscopy," *Biomedical Engineering, IEEE Transactions on*, vol. 53, no. 4, pp. 762–766, 2006.

[7] C. De Hauwer, F. Darro, I. Camby, R. Kiss, P. Van Ham, and C. Decaesteker, "In vitro motility evaluation of aggregated cancer cells by means of automatic image processing," *Cytometry*, vol. 36, no. 1, pp. 1–10, 1999.

[8] D. Padfield, J. Rittscher, N. Thomas, and B. Roysam, "Spatio-temporal cell cycle phase analysis using level sets and fast marching methods," *Medical image analysis*, vol. 13, no. 1, pp. 143–155, 2009.

[9] F. Bunyak, K. Palaniappan, S. K. Nath, T. I. Baskin, and G. Dong, "Quantitative cell motility for in vitro wound healing using level set-based active contour tracking," in *Biomedical Imaging: Nano to Macro, 2006. 3rd IEEE International Symposium on*. IEEE, 2006, pp. 1040–1043.

[10] E. C. Sherbrooke, N. M Patrikalakis, and E. Brisson, "An algorithm for the medial axis transform of 3d polyhedral solids," *Visualization and Computer Graphics, IEEE Transactions on*, vol. 2, no. 1, pp. 44–61, 1996.

[11] H. Abdi, "Partial least squares regression and projection on latent structure regression (pls regression)," *Wiley Interdisciplinary Reviews: Computational Statistics*, vol. 2, no. 1, pp. 97–106, 2010.